Formation of laser-induced periodic surface structures on reaction-bonded silicon carbide by femtosecond pulsed laser irradiation

WCMNM 2021

Tushar Meshram[1] Jiwang Yan[1,*]

[1] *Department of Mechanical Engineering, Keio University*
3-14-1, Hiyoshi, Kohoku, Yokohama, Kanagawa 223-8522, Japan
** yan@mech.keio.ac.jp*

Abstract

Reaction-bonded silicon carbide (RB-SiC) is an excellent engineering material with high hardness, stiffness, and resistance to chemical wear. However, these properties make it difficult to process RB-SiC, especially making micro/nanoscale functional surface structures on it by mechanical and chemical methods. In this study, fundamental characteristics of laser-induced periodic surface structures (LIPSS) on RB-SiC by femtosecond pulsed laser irradiation were investigated. Low spatial frequency LIPSS (LSFL) and high spatial frequency LIPSS (HSFL) formed perpendicularly to the laser polarization direction. Under specific laser fluence and scanning speed, HSFL-LSFL hybrid structures were observed on SiC grains. It was also observed that the direction of laser scanning with respect to laser polarization direction affected the uniformity of generated LIPSS. Raman spectroscopy was performed to identify the material composition of the LIPSS. Finally, the surface wettability test showed that the formation of LIPSS made the surface superhydrophilic with a contact angle of less than 8°. The proposed method was demonstrated to be an effective approach to fabricate periodic micro/nanostructures over a large area to modify the surface properties.

Keywords: reaction-bonded silicon carbide, surface texturing, two-phase material, femtosecond pulsed laser

1. Introduction

Reaction-bonded silicon carbide (RB-SiC) is an excellent engineering material with high hardness, stiffness, and is resistant to chemical wear, thus it is widely employed in various industrial applications requiring high wear and corrosion resistance. Due to its high thermal conductivity and low coefficient of thermal expansion, RB-SiC components are widely used in thermal management or heat dissipation applications such as high voltage power supply, heat exchanger tubing, etc. RB-SiC is also used as molds in a wide variety of applications such as manufacturing glass lenses by compression molding, optical mirrors, and even structural components.

However, processing RB-SiC has some unique difficulties, the material properties which make it such a desirable material also make it very difficult to process by mechanical and chemical methods. Furthermore, RB-SiC consists of two different phases, SiC grains in a Si matrix. Si and SiC have very different mechanical, chemical properties which adds to the complexity of processing RB-SiC and makes it difficult to generate uniform surface structures. There is a growing demand for micro and nanostructured surface in various industrial applications, as the generation of these structures can drastically improve and enhance the desirable surface properties such as reflectivity, heat dissipation, friction coefficient, and wettability.

Laser processing can be a very effective method of creating such surface structures, as laser is a non-contact process hence is not affected by hardness and chemical inertness of material. In the past decade, laser-induced periodic surface structures (LIPSS) have been extensively studied to create functional surfaces. There are previous researches on LIPSS formation on Si and SiC, but no studies have been reported on LIPSS formation on RB-SiC as per the authors' best knowledge. Si and SiC have different optical properties and bandgaps, and thus they interact differently with the same laser. Hence understanding laser interaction with this two-phase material will be crucial for creating functional surfaces to meet the current demand of textured surfaces and would boost widespread use of RB-SiC in the industries.

Hence in this paper, we investigated fundamental characteristics of LIPSS formation on RB-SiC by femtosecond pulsed laser irradiation. Change in the material composition of the surface after LIPSS formation was also evaluated. In addition, we examined the change in surface wettability due to LIPSS formation.

2. LIPSS formation mechanism for RB-SiC

LIPSS can be divided into two categories based on the period (Λ) [1]. The first category is, when the period of LIPSS is near to the wavelength of laser ($\Lambda_{LSFL} \sim \lambda$), called low spatial frequency LIPSS (LSFL), which are mostly known to form on highly absorptive materials. The most widely accepted mechanism for LSFL formation is the interaction of laser with surface electromagnetic waves (SEW) [2], which results in selective ablation of the surface. The second category is, when the LIPSS period is much smaller than the wavelength of laser ($\Lambda_{HSFL} << \lambda$), called high spatial frequency LIPSS (HSFL) and known to form on weak absorptive materials. Even though the exact mechanism is still under debate, HSFL are usually attributed to the generation of surface plasmon polaritons (SPP), material self-organization and

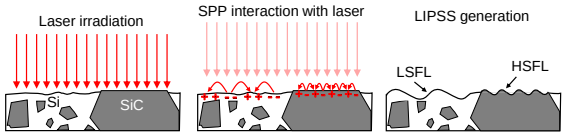

Fig. 1 Mechanism of LIPSS formation on RB-SiC.

second harmonic generation [3, 4].

It is thought that LIPSS generation on RB-SiC is due to the generation of SPP (Fig. 1). While ideally, SPP can only propagate between metal and dielectric interface, SPP can be generated on semiconductors by laser irradiation. When semiconductors are irradiated with ultrashort pulses, a lot of free electrons are generated near the surface of the semiconductor thus attaining a metal-like state [5, 6]. However, the number of electrons that will be generated is affected by the bandgap of the semiconductor. Thus, in the case of RB-SiC, a lower electron density is generated on SiC (3.023 eV) as compared to Si (1.1 eV). This difference in generated electron density coupled with the difference in permittivity results in the formation of SPP with a different period on SiC as compared to Si (Fig. 1). As laser interacts with generated SPPs, it creates a different interference pattern on SiC than that on Si, resulting in the formation of LSFL on Si and HSFL on SiC.

3. Experimental procedures

The RB-SiC sample used in this research was cylindrical with a diameter of 50 mm and a height of 15 mm. In Raman spectroscopy of the sample surface, the Si matrix showed a Raman peak for single crystal silicon, while SiC grains showed a Raman peak of 6H-SiC. The laser used in the experiments was PHAROS-08-600-PP manufactured by Light Conversion, Lithuania. The laser had a wavelength of 1030 nm and could create ultra-short pulses with a width of 256 fs with a pulse frequency of 100 kHz. The laser scanning was controlled using a galvanometer scanning system and laser was focused on the sample using an f-theta lens. The focused spot had a diameter of ~20 µm with a gaussian distribution. All the experiments in this study were carried out in atmospheric conditions at room temperature (~23 °C). Other laser parameters are shown in Table 1. After the experiment, the irradiated surface was cleaned with ethanol and was observed using a field emission scanning electron microscope (FE-SEM). Depth at which LIPSS formed was measured by Optical microscope OLS 4000 by Olympus Co., Japan. The material composition was characterized using Raman spectroscopy.

Table 1
Experimental conditions

Laser medium	Yb : KGW
Wavelength [nm]	1030
Spot size [µm]	20
Pulse width [fs]	256
Repetition frequency [kHz]	100
Scanning speed [mm/s]	10, 20, 40, 60, 80, 100
Scanning pitch [µm]	15, 40
Laser fluence [J/cm^2] (Energy per pulse/spot area)	0.16, 0.32, 0.48, 0.63, 0.95, 1.27, 1.59
Number of scans (N)	1, 5

4. Results and discussion

4.1. Effect of laser fluence

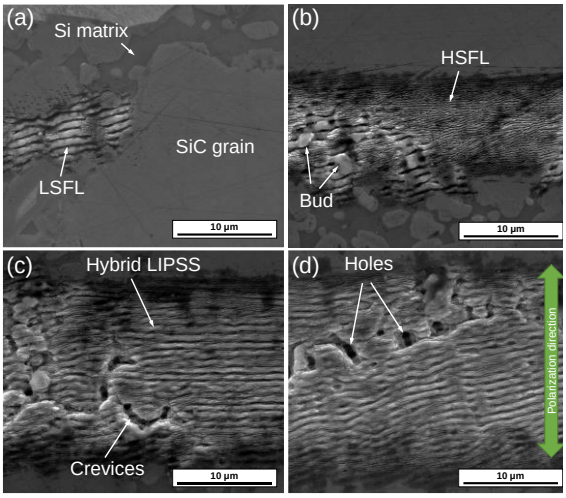

Fig. 2 SEM images of line irradiation at a scanning speed of 60 mm/s and fluence of (a) 0.16, (b) 0.32, (c) 0.95, and (d) 1.59 J/cm^2.

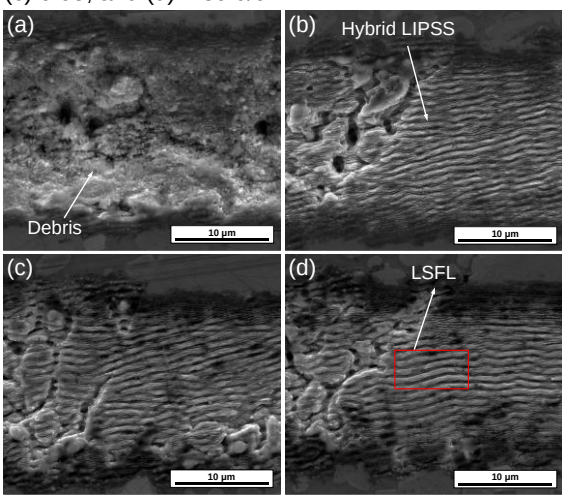

Fig. 3 SEM images of line irradiation with a fluence of 0.95 J/cm^2 and scanning speed of (a) 10, (b) 40, (c) 80, and (d) 100 mm/s.

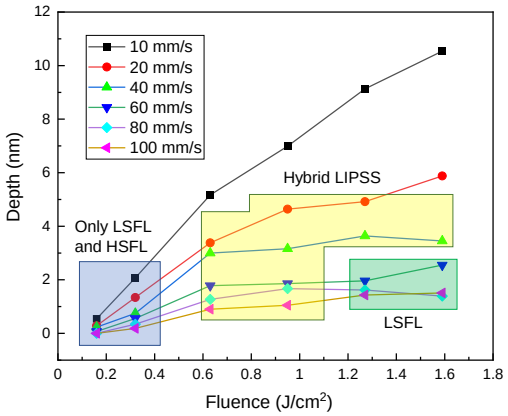

Fig. 4 Type of LIPSS formation at various laser fluence and scanning speeds.

Line irradiation was carried out to observe the effect of laser fluence on LIPSS formation, laser scanning speed was 60 mm/s and N = 1. The scanning direction was perpendicular to the polarization direction. The SEM images of LIPSS formed at various fluence are shown in Fig. 2. When fluence was 0.16 J/cm^2, LSFL with a period of 850 ± 25 nm were

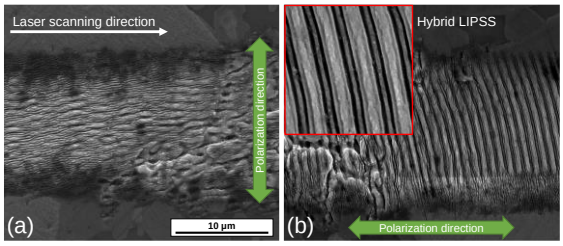

Fig. 5 SEM images of line irradiation with laser scanning direction (a) perpendicular and (b) parallel to the laser polarization direction.

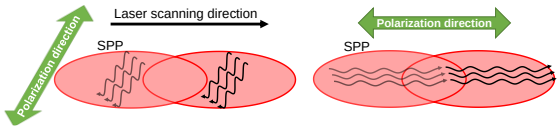

Fig. 6 Schematic diagram of the direction of SPP formation.

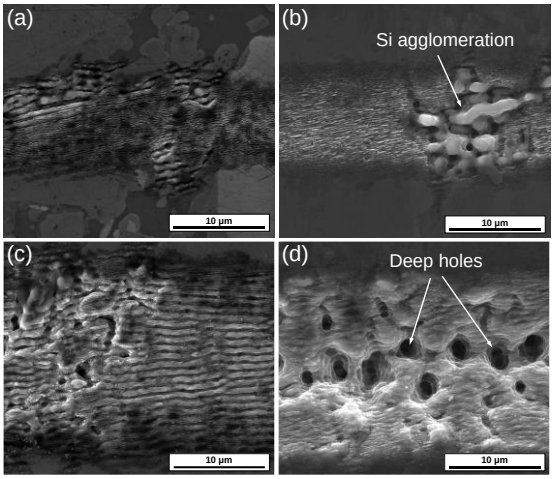

Fig. 7 SEM images of line irradiation when laser was scanned (a), (c) 1 and (b), (d) 5 times.

observed on Si matrix, and no LIPSS structures were observed on SiC grains. As the fluence was increased to 0.32 J/cm^2, LSFL structures on Si combined to form bud shapes whereas HSFL with a period of 175 ± 25 nm were observed on SiC grains. Both LSFL and HSFL formed perpendicular to the direction of laser polarization. The reason for LIPSS formation with a different period on Si and SiC is because the energy of laser photons (1.2 eV) used in this research is close to the bandgap of Si (1.1 eV), thus Si shows a high absorptivity coefficient for this wavelength. However, SiC is a high bandgap (3.023 eV) semiconductor and has a very low coefficient of absorption for the used laser wavelength.

As fluence was further increased (Fig. 2c, 2d), it was observed that Si regions were significantly ablated, resulting in the formation of crevices and holes. Whereas in the case of SiC grains, HSFL structures agglomerate to form LSFL in the centre, while only HSFL structures occur near the boundary. This transformation of HSFL into LSFL is thought to be the result of thermal decomposition of SiC into Si and C. In Fig. 2d, the HSFL-LSFL hybrid structures did not form and only LSFL is observed.

4.2. Effect of laser scanning speed

Line irradiation was carried out for various speeds

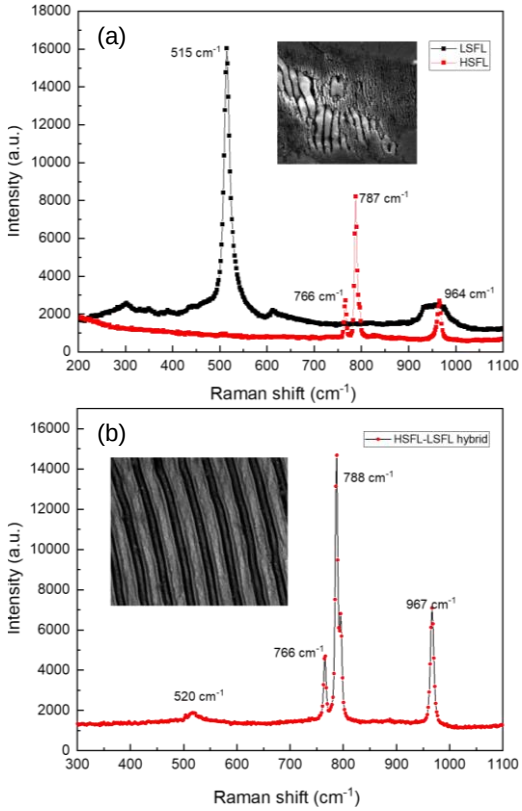

Fig. 8 Raman spectroscopy analysis of (a) regular and (b) hybrid LIPSS.

with a fluence of 0.95 J/cm^2 and N = 1. Fig. 3 shows the SEM images of LIPSS formation. At 10 mm/s, there was almost no sign of LIPSS formation. Instead, a was groove formed on the surface. The groove wall was covered with fine granular structures which are thought to be reattached debris after laser irradiation. At 40 mm/s, HSFL-LSFL hybrid structures can be observed with holes formed in Si matrix regions. In Fig. 3c and 3d, it can be observed that the HSFL-LSFL hybrid structures are converted to LSFL. This is because at lower scanning speed, due to the high pulse overlap rate, Si is vaporized thus generating hybrid LIPSS. However, at higher scanning speed, the pulse overlap rate decreases, and thus LSFL structures are formed. Fig. 4 shows range of fluence and scanning speed at which different types of LIPSS form. For all scanning speed conditions at low fluence, LSFL and HSFL formed separately as shown in Fig. 2b. As fluence is increased, LIPSS did not form at lower speeds, while hybrid LIPSS formed as shown in Fig. 3b and 3c. Even though the hybrid LIPSS look similar, the depth at which they form for a given fluence is dependent on scanning speed. At high fluence and high scanning speed, the hybrid LIPSS did not form, instead only LSFL was observed.

4.3. Effect of laser scanning direction

Fig. 5 shows SEM images after laser was irradiated in parallel (Fig. 5b) and perpendicular (Fig. 5a) direction to the laser polarization direction. Laser fluence was 0.63 J/cm^2. The scanning speed was 100 mm/s and N = 1. Both the images show HSFL-LSFL hybrid structures. However, the LIPSS structures in Fig. 5b are parallel to each other, ordered and more uniform as compared to Fig. 5a, suggesting the

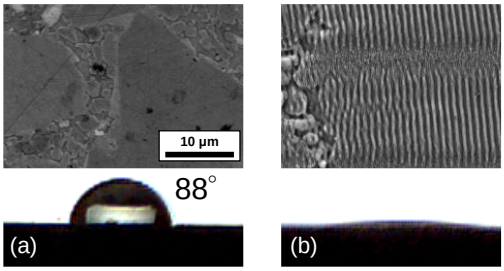

Fig. 9 Water droplet on (a) original surface and (b) after hybrid LIPSS formation.

intensity of SPP when laser was scanned parallel to polarization direction was much stronger. It is thought that this inconsistency is due to the formation and decay of surface plasmon polariton (SPP). As presented in Fig. 6, when the laser is scanned perpendicular to the direction of polarization, the generated SPP is parallel to the polarization direction (for Si, SiC). As the laser moves ahead the SPP is generated in a new location and previously generated SPP decays, which leads to non-uniformity of the SPP in the laser movement. While, in the case when the laser is scanned parallel to the polarization direction, the generated SPP is in the same direction as laser movement, and hence excitation and propagation of SPP is assisted by subsequent SPP generation [7, 8]. This leads to the formation of much more uniform LIPSS.

4.4. Effect of scanning repetition

Fig. 7 shows SEM images of surfaces line-irradiated with a scanning speed of 100 mm/s and N = 1, 5. At a low fluence of 0.32 J/cm^2 (Fig. 7a, 7b), the increase in scanning repetition caused Si to melt and agglomerate. This is thought to be because laser fluence can melt silicon but is not enough to vaporize it, thus leading to agglomeration of molten silicon. Slight ablation occurred on the SiC grains but HSFL structures remained on the surface. At a high fluence of 1.62 J/cm^2 (Fig. 7c, 7d), an increase in scanning repetition led to the complete removal of Si from the surface, which resulted in the formation of deep holes. It was also observed that, due to ablation of SiC grains the LSFL structures become less defined and shallower.

4.5. Material analysis of LIPSS

Fig. 8 shows Raman spectra of LSFL, HSFL, and HSFL-LSFL hybrid structures. Line irradiation was carried out with a scanning speed of 10 mm/s and fluence of 0.16 J/cm^2. Raman shift obtained for LSFL was 515 cm^{-1} which was near the Raman shift of single crystal Si, whereas HSFL structures showed a Raman shift of 6H-SiC. Thus, the result confirms that LSFL structures are formed in Si matrix region and HSFL on SiC grains. However, Raman shift for HSFL-LSFL hybrid structures also showed a Raman shift of 6H-SiC, although a small peak of Si can be observed around 520 cm^{-1}. It was expected that a much stronger intensity of Raman peak for Si would be observed, as the LSFL structure covers most of the surface in the hybrid LIPSS structure, this could be because hybrid LIPSS structures formed on SiC grain.

4.6. Surface wettability change

The wettability of the surface before and after hybrid LIPSS generation was measured. The sample was prepared by parallel line irradiations with a pitch of 15 µm within an area of 5 mm × 5 mm, scanning speed was 100 mm/s, and N = 1. Under these conditions, SiC grains were mostly covered with hybrid LIPSS as shown in Fig. 9b Static sessile drop method was used to measure the contact angle of distilled water with the surface. The contact angle with the original surface was around 88° (Fig. 9a) but after LIPSS formation the surface became hydrophilic and the contact angle was reduced to less than 8° (Fig. 9b).

5. Conclusions

Femtosecond pulsed laser irradiation was carried out on RB-SiC to investigate fundamental characteristics and conditions for LIPSS formation. It was found that at low fluence LSFL (Λ_{LSFL}) formed on Si and HSFL (Λ_{HSFL}) on SiC. At medium and high fluence Si matrix was ablated at a much higher rate than SiC grains resulting in the formation of deep holes on the surface. An increase in laser scanning speed at medium and high fluence led to the formation of HSFL-LSFL hybrid LIPSS. Laser scanning direction with respect to the polarization of laser affected the uniformity of generated LIPSS structures. Furthermore, the formation of LIPSS on RB-SiC made the surface hydrophilic.

References

[1] J. Bonse et al., “On the role of surface plasmon polaritons in the formation of laser-induced periodic surface structures upon irradiation of silicon by femtosecond-laser pulses,” J. Appl. Phys., 2009;106(10).
[2] G. Miyaji et al., “Origin of Periodicity in Nanostructuring on Thin Film Surfaces Ablated with Femtosecond Laser Pulses,” Opt. Express., 2008; 16(20): pp. 16265-16271.
[3] A. Borowiec et al., “Subwavelength Ripple Formation on the Surfaces of Compound Semiconductors Irradiated with Femtosecond Laser Pulses,” Appl. Phys. Lett., 2003; 82(25): pp. 4462–4464.
[4] D. Dufft et al., “Femtosecond Laser-Induced Periodic Surface Structures Revisited: A Comparative Study on ZnO,” J. Appl. Phys., 2009; 105(3): pp. 034908.
[5] M. Huang et al., “Origin of Laser-Induced near-Subwavelength Ripples: Interference between Surface Plasmons and Incident Laser,” ACS Nano., 2009; 3(12): pp. 4062–4070.
[6] D. Puerto et al., “Femtosecond Laser-Controlled Self-Assembly of Amorphous-Crystalline Nanogratings in Silicon,” Nanotechnology, 2016; 27(26).
[7] V.V. Gerasimov et al., “Surface Plasmon Polaritons Launched Using a Terahertz Free-Electron Laser: Propagation along a Gold–ZnS–Air Interface and Decoupling to Free Waves at the Surface Edge,” J. Opt. Soc. Am. B, 2013; 30(8): pp. 2182-2190.
[8] W. Liu et al., “Manipulation of LIPSS Orientation on Silicon Surfaces Using Orthogonally Polarized Femtosecond Laser Double-Pulse Trains,” Opt. Express., 2019; 27(7): pp. 9782- 9793.